Exploration of Model Updating Methods Based on GVT of a Blended Wing Body Configuration Aircraft

Hugo Miguel Candeias Faustino
hugomcfaustino@tecnico.ulisboa.pt

Instituto Superior Técnico, Universidade de Lisboa, Portugal

November 2021

Abstract

The high standards the aerospace industry has to meet imply validation of concepts and designs by thoroughly testing them. This work focuses on Ground Vibration Testing, which is carried out on a Blended Wing Body concept and the data extracted used to update structural parameters of simplified Finite Element Models. The study was conducted at University of Victoria's Centre for Aerospace Research. Prior to testing phase, an introductory Model Update analysis was done using *FEMtools* on previously obtained experimental results for the aircraft's wing. A user interface to extract data from the test sessions was done in *LabVIEW* and a model to animate and extract modal parameters from was created in *MEscope*. The Modal Analysis results were then used to match the frequency and mode shapes between the experimental and an analytical simplified model of the aircraft. Two sessions of Ground Vibration Tests were performed to collect all the needed data and proceed with the model updating study. This time, the frequency matching was made recurring to *FEMtools* but the dynamic mode shape study was done through an optimization algorithm developed in *MATLAB*. A relatively simple beam Finite Element Model was generated and proved to accurately match the natural frequencies obtained experimentally. More complex models were then produced to mimic the mode shapes, which proved to be challenging.
Keywords: Ground Vibration Testing, Finite Element Models, Model Update, Modal Analysis.

1. Introduction

Among promising configurations for air vehicles regarding aerodynamic efficiency one has the Blended Wing Body (BWB), and despite technical challenges on some areas of its design (namely on its stability and control), this concept also trumps the conventional aircraft when considering noise levels, weight and operating costs. Having the fuselage and wings combined into one smooth shape instead of three distinct parts assembled, the hybrid design resembles a flying wing, albeit incorporating features of conventional aircraft [1]. Its lift to drag ratio is higher due to the reduced ratio of wetted area over reference area, representing a breakthrough in subsonic transport efficiency [2].

The University of Victoria Centre for Aerospace Research (UVic CfAR), on behalf of Bombardier Aerospace (BA), is responsible for the design, building and testing of a BWB prototype scaled at 16.5%.

As the project unraveled, the need for performing Ground Vibration Tests (GVTs) on the aircraft emerged for both validation purposes and so that its structural dynamic models could be improved. These models are then used to study flutter behavior and to plan flight tests. Being performed late in the development cycle and when the availability of the aircraft is limited, the pressure to get the test results as efficiently as possible without compromising the accuracy of the results is quite high.

For the purpose of this study, GVT is to be conducted on the aircraft and computational tools are used in an attempt at describing its dynamic responses through a Finite Element Model (FEM). The focus here is on trying to optimize a simplified model made of beam elements and lumped masses instead of a complete FEM so that a study of how little freedom can be given to a model that still is able to correctly mimic reality can be performed.

During GVT, it is important to accurately identify the first natural frequency happening on the aircraft's structures. This has to do with the fact that frequencies lower than the ones previously analytically predicted may compromise the behavior of the autopilot's filters. As for the model updating, the frequency is to be matched in the first place. Once an optimized solution has been found for this, the study follows with the matching of mode shapes.

2. Background

Dynamic aeroelasticity, consisting in the interaction between elastic, inertial and aerodynamic forces, is to be studied during the design and optimization phases for any aircraft.

2.1. Modal Analysis

Modal analysis is the process of exploring the inherent dynamic characteristics of a system in terms of its natural frequencies, damping factors and mode shapes with the main goal of formulating a mathematical model for studying its dynamic behavior.

When excited at one of its natural frequencies, any structure vibrates and deforms in what is called mode shape. Under typical working conditions, a structure vibrates in a compounded combination of all mode shapes overlaid [3]. Therefore, the complete understanding of the potential ways a structure can vibrate is only acquired when one identifies every mode shape.

Quantification of modal parameters is possible through measurements of Frequency Response Functions (FRFs) during modal testing, which involves three main phases: test preparation, frequency response measurements and modal parameter identification.

2.1.1 Eigenvalues and Eigenvectors

For the general damped case, the complete Newton's equation for a vibrating system with Multiple Degrees of Freedom (MDOFs) can be modeled as a second order differential equation:

$$M\ddot{\boldsymbol{u}} + C\dot{\boldsymbol{u}} + K\boldsymbol{u} = \boldsymbol{f}, \tag{1}$$

where M, C and K are respectively the mass, damping and stiffness matrices and $\boldsymbol{u}$, $\dot{\boldsymbol{u}}$ and $\ddot{\boldsymbol{u}}$ are the displacement, velocity and acceleration for each Degree of Freedom (DOF) of the modeled system. The equation adds up to the external excitation $\boldsymbol{f}$. If f is set to equal 0, one can solve for the eigenvalues and eigenvectors after some manipulation, getting

$$s_i = -\zeta_i\omega_i + j\omega_i\sqrt{1-\zeta_i^2} \tag{2}$$

for $i = 1, 2, ..., N$. In this equation ω_i represents the angular natural frequencies and ζ_i the damping.

2.1.2 Frequency Response Function

For a linear system, a Transfer Function (TF) can be defined as the ratio between the Laplace Transform of the output $Y(s)$ and the Laplace Transform of the input $X(s)$:

$$H(s) = \frac{Y(s)}{X(s)} = \frac{\text{Laplace Transform of } y(t)}{\text{Laplace Transform of } x(t)}. \tag{3}$$

The FRF is obtained by evaluating the TF on the imaginary axis in the Laplace domain where $s = i\omega$ and can be represented in terms of amplitude and phase or in terms of real and imaginary parts. The amplitude represents the ratio between the input force and the response while the phases diagram gives information on whether the motion of the structure is happening in or out of phase with the input.

Including sufficient points while testing is of extreme importance to thoroughly describe the modes of interest. Moreover, a mode of vibration can be excited at any point of the structure as long as not in a nodal point [4].

The natural frequencies are identified by the peaks appearing at the same frequency at every measurement point and these amplitudes combined describe the mode shape for the corresponding natural frequency. The damping, on the other hand, can be determined by the half-power method, which quantifies the sharpness of each resonant peak [5] — the wider a peak is, the higher the damping [3].

2.2. Ground Vibration Tests

GVT is performed at the integrated aircraft level and conducted to fulfill requirements imposed by certification authorities. Choosing both the data acquisition system and excitation techniques also play an important role when worried about the efficiency of the test. The answer to questions like 'how many accelerometers should be used?', 'where should they be placed on the structure?', 'how should the aircraft be supported to simulate a free-free condition and so that the first flexible mode is well separated from the rigid body modes?' needs to be well established before moving to the testing phase.

The first step in modal analysis experiments is measuring both the excitation and responses of the structure being tested. The structure is to be excited and the applied excitation force, as well as the resulting response vibrations — accelerations — are measured, resulting in a FRF data set.

2.2.1 Shaker Testing vs. Impact Testing

The excitation function dictates the choice of the excitation system and the reverse is also true.

Commonly used shakers for modal analysis are electromagnetic and the electro-hydraulic ones. For the electromagnetic shaker, force is generated by a magnetic coil driven by alternating current.

The impact hammer is another excitation mechanism. Providing shorter measurement time and requiring little hardware, it is a simpler technique. Since the amplitude level of the energy to be applied to the structure depends on its linear momentum and the hammer's velocity is difficult to control,

the force level is usually controlled by varying the mass. Mass can be added to or removed from the majority of hammers, making them useful for testing on a different range of objects of different sizes and weights.

Shakers allow more control over the excitation force and also sample more information than the hammer per unit of time, since they are able to apply more energy to the structure for longer. On the other hand, the fact that no mass is attached nor extra stiffness applied to the structure is a clear advantage of the impact hammer. Even though the hammer is a more expedite alternative, both methods share the fact that the setup time takes longer than the test time itself.

Due to the equipment already available at CfAR and expensive costs associated with buying a modal shaker, the methodology chosen for GVT was the one using an impact hammer. The DOFs in impact hammer testing correspond to places marked along a structure where data is collected.

The task of selecting sensor placement and hammer taps can be eased by previously analyzing the FEM of the aircraft so that DOFs do not coincide with nodes of the mode shapes of interest.

When choosing to perform a modal test with an impact hammer on a structure without as many accelerometers as the number of DOFs, one has to decide whether to rove the accelerometers or to rove the hammer.

The roving accelerometer technique implies moving the sensor while the excitation source remains at the same point, whereas the roving hammer method implies the fixing of the sensor at a certain point and the excitation source to move from DOF to DOF in which the FRF is to be measured. The need to unmount and remount sensors over all the DOFs in the roving accelerometer method would be a major drawback and would take much longer than roving the hammer. Given the equivalence between both methodologies from a physics point of view, the latter was chosen.

2.3. Finite Element Model Updating

The purpose of model updating is to study how changes in a structure's design influence its response. This process ensures problems such as manufacturing weight differences, flawed boundary conditions definition and incorrect assumptions on properties of the materials are reckoned.

The software used to explore the model updating process throughout this study was initially *FEMtools*. For mode shape model updating of the aircraft in which GVT was performed, an optimization algorithm developed in *MATLAB* was also used.

2.3.1 Modal Assurance Criterion

The Modal Assurance Criterion (MAC), bounded between 0 — indicating inconsistency — and 1 — indicating fully consistent mode shapes — is used to compare mode shapes obtained experimentally with the ones derived from analytical models. Mathematically one has:

$$\mathrm{MAC}(\psi_a, \psi_e) = \frac{\left|\{\psi_a\}^T\{\psi_e\}\right|^2}{\left(\{\psi_a\}^T\{\psi_a\}\right)\left(\{\psi_e\}^T\{\psi_e\}\right)}, \quad (4)$$

where ψ_a is the analytical modal vector and ψ_e is the experimental modal vector.

MAC information is presented through either a 2D or 3D plot, where discrete mode to mode comparison is shown. Despite being a great tool as an assurance indicator, it can only indicate consistency, not validity nor orthogonality [6]. Therefore, attention should be paid while making use of this criterion. Values of MAC above 0.9 were considered as well correlated while values bellow 0.6 were considered with caution because they may or may not indicate correlation and therefore lack of resemblance.

2.3.2 Correlation Coefficients

Correlation Coefficients (CCs) are chosen to be minimized during the FEM updating. For this study, the most important CCs to be used when model updating are CCABS when focused on the convergence of modal frequencies, CCMAC when trying to converge the MAC and CCTOTAL when a broader convergence is the preferable option.

CCABS measures the absolute relative difference between resonance frequencies:

$$\mathrm{CCABS} = \frac{1}{N}\sum_{i=1}^{N}\frac{|\Delta f_i|}{f_i}. \quad (5)$$

CCMAC measures the difference between target and average actual MAC:

$$\mathrm{CCMAC} = 1 - \frac{1}{N}\sum_{i=1}^{N}\mathrm{MAC}_i. \quad (6)$$

CCTOTAL is the total CC value and accounts for frequency, mass, displacement and MAC correlation coefficients.

When performing a new iteration, *FEMtools* automatically verifies the values of the CC and checks if a convergence criterion has been satisfied, stopping the iteration loop if either $\mathrm{CC}_t < \varepsilon_1$ or $|\mathrm{CC}_{t+1} - \mathrm{CC}_t| < \varepsilon_2$, where CC_t is the reference CC at iteration t and $\varepsilon_{1,2}$ are imposed margins [7].

3. Beam Finite Element Model Updating

During his masters thesis, Araújo [8] performed GVTs on the right wing of the BWB aircraft. After the test phase, an attempt at model updating based on frequencies and mode shapes was made. At the end of his study, matching of frequencies was successful but when trying to match mode shapes no convergence was reached. For that reason, a higher complexity FEM was created with more freedom to change parameters when model updating.

3.1. Beam Model

This FEM was developed using *Ansys APDL* capabilities. After several iterations, the chosen model is the one presented in Fig.1, featuring 74 beam elements and 75 lumped masses.

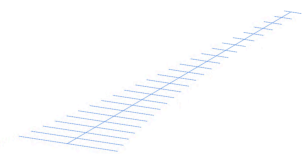

Figure 1: New wing simplified FEM.

The wing's root was fixed for all DOFs in order to simulate the conditions in which tests had been performed. The natural frequencies of the FEM from *Ansys* are shown in Table 1 and compared with the Experimental Modal Analysis (EMA) ones.

Table 1: Natural frequencies for FEM and EMA.

Mode #	f_{EMA} (Hz)	f_{FEA} (Hz)	Δ_f (%)
1	10.34	4.11	-60.23
2	35.28	22.92	-35.03
3	50.38	29.90	-40.65
4	81.34	61.95	-23.84
5	129.80	120.09	-7.48
6	142.72	165.63	16.05
7	157.48	196.95	25.06

3.2. FEMtools Model Updating

Matching of EMA DOFs and nodes from the FEM allowed one to compute CCABS and CCMAC and study how the change in some parameters influenced the structure's behavior. The parameters to set free to change during model updating included the Young's Modulus E, mass density ρ, cross section area A, torsional stiffness I_x, bending moments of inertia $I_{y,z}$ and lumped masses m_G.

3.2.1 Updating Based on Frequencies

With focus on the frequencies, the CC to be used was CCABS — initially at 29.5%. As for the convergence criteria, the margin ε_1 was selected to be 1 and the margin ε_2 was chosen as 0.1.

The initial attempts were:

- Updating of E.
- Updating of E and ρ.
- Updating of E, ρ and m_G.
- Updating of E, ρ, A and m_G.
- Updating of E, ρ, A, I_x, I_y, I_z and m_G.

The results obtained for CCABS are presented in Table 2.

Table 2: Comparison of CCABS after different model updates.

Update of	$\text{CCABS}_{\text{final}}$ (%)
E	16.7
E, ρ	15.8
E, ρ, m_G	16.0
E, ρ, A, m_G	6.0
$E, \rho, A, I_x, I_y, I_z, m_G$	0.72

When introducing m_G, the number of Design Variables (DVs) grew by but the final CCABS was lower than the one where only E and ρ were updated. However, this happened at a lower overall number of iterations, meaning that the global number of parameter updates performed by *FEMtools* was lower for the case where m_G was introduced.

With a CCABS lower than 1, the last attempt showed to be successful. However, an update of a lower number of DVs is attempted, taking into account the results gotten so far.

Both m_G and I_x were not considered for this final try given the low impact they are predicted to have on the final result. Adding to that, the 7th mode shape is also not paired in this attempt due to the lack of understanding on what is happening in the experimental mode shape — which can suggest the presence of errors on either the data acquisition or post processing of data.

Starting with a CCABS of 31.6%, using E, ρ, A, I_y and I_z as parameters to be updated, the model updating process converged after just 3 iterations to a value of $\text{CCABS}_{\text{final}} = 0.69\%$. Results can be seen in Table 3.

As expected, by disregarding the 7th mode shape, not only was the final CCABS lower but it also took less iterations to reach convergence. Similarly, the reduction on the number of DVs did not contribute to a higher number of iterations before convergence nor did it jeopardize the final result.

Table 3: Results obtained for a last model update based on frequencies.

Mode #	f_{EMA} (Hz)	$f_{\text{FEA}_{\#6}}$ (Hz)	Δ_f (%)
1	10.34	10.36	0.19
2	35.28	34.86	-1.19
3	50.38	49.51	-1.73
4	81.34	81.21	-0.16
5	129.80	129.93	0.10
6	142.72	143.91	0.83

3.2.2 Updating Based on Mode Shapes

Since the focus now was on a broader aspect of modal analysis, the CC chosen to be converged while model updating was the CCTOTAL. The mode shape pairing was performed in a sequential order, meaning that the 1st mode shape obtained from EMA is paired with the 1st mode shape from FEA and so on as seen in Table 4.

Table 4: Initial MAC values for mode shape pairs.

EMA mode #	FEA mode #	MAC (%)
1	1	97.0
2	2	73.2
3	3	32.7
4	4	39.2
5	5	1.5
6	6	2.3
7	7	0.5

Due to very low initial MAC values for pairs #5, #6 and #7, the initial focus will lie on the matching of the 1st, 2nd, 3rd and 4th mode shape pairs.

3.2.3 CCTOT convergence

Similarly to the frequency matching, different combinations of parameters were chosen to update:

- Updating of E.
- Updating of E and ρ.
- Updating of E, ρ, A, I_y and Iz.

After running *FEMtools*, CTOT was reduced from 80.01% to 50.02%, 50.76% and 42.35% for each of the three different attempts respectively. Although apparently converging, CCMAC did not reduce its value in any of the model updates. Instead, *FEMtools* converged CCABS. For that reason, CCMAC was then attempted to converge, letting the natural frequencies adjust freely.

3.2.4 CCMAC convergence

Using the same sets of parameters, CCMAC was attempted to converge.

Initially at 39.44%, CCMAC converged to 39.41%, 39.93% and 41.59% respectively. Once again, *FEMtools* was not able to approximate the behavior of the simplified FEM to the wing. Instead, the software appears to match the frequencies, even when no constraint was applied to them.

These results lead one to think that either a simplified model constituted by beams and lumped masses is not ideal for describing a wing's behavior and therefore there is no solution for the problem as it was formulated or that the software itself is incapable of performing the required task without being biased towards matching the frequencies over matching the mode shapes.

4. Experimental Testing and Data Post-Processing Procedures

As preparation for GVT on the assembled aircraft, tests on a wing structure specimen were performed.

4.1. Data Acquisition Equipment and Software

The equipment used for the tests described in the current and following chapters include:

- One ICP Impact Hammer Model 086C03. The soft hammer tip was selected since the range of frequencies of interest does not extended to higher frequencies than 150-200Hz.
- One IEPE NI 9234 acquisition card, to which the hammer and accelerometers connect.
- Two PCB Piezotronics Accelerometers Model 352A24, placed in such a way they collect both in-plane and out-of-plane information depending on the direction of the hammer hit.
- One rope for hanging the wing. The frequencies at which the RBM oscillations appear depend on the length of the rope but the natural frequencies do not. For this reason, it can be varied in order to shift them if found necessary.

The free-free boundary condition was simulated by hanging the wing by a rope from above. Even if not an ideal free-free scenario, the mode shapes remain unchangeable as long as there is no overlapping of the RBMs with elastic deformations on the FRF spectra.

A *LabVIEW* interface was developed in order to collect the information coming from both the impact hammer and the two sensors through the DAS. Each FRF is saved in a .uff file format containing its real and imaginary parts. The averaging of three successful impacts is then to be obtained for every recording. The recording is only to be saved and

further analyzed when the coherence for the frequency range of interest is above 0.9. If not, the recording of another three successful impacts is to be redone for that same DOF.

4.2. Wing Specimen GVT

Divided throughout the leading and trailing edges, 18 points were chosen to hit during this test. Given the geometry of the wing, the 9 points on the leading edge could be tested for both out-of-plane and in-plane vibration modes, while the remaining ones on the trailing edge were tested for in-plane vibrations only.

In Fig.2 one can see the simplified model created on *MEscope* for the wing specimen. No data is extracted at this location and for that reason the software's interpolation capabilities may be used when visualizing the mode shapes for point 19.

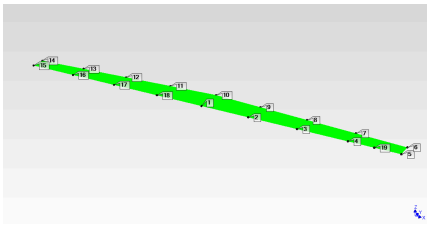

Figure 2: *MEscope* model for the wing specimen.

Once all FRFs were collected, the model generated on *MEscope* was animated. To do so, each of the FRF had to be associated to the specific DOF where the hammer had hit while taking into account which sensor had collected that FRF.

4.2.1 Modal Parameters Extraction

After examining the spectra of the FRFs one can easily predict and approximate the structure's resonant frequency. Nonetheless, mathematical algorithms present in the software allow a more accurate approximation for the natural frequencies and damping.

Presented in Table 5, the modal parameters extracted using *MEscope* capabilities correspond to eight out-of-plane mode shapes — #1 to #6, #9 and #10 — and two in-plane mode shapes — #7 and #8.

Even though there are peaks located at frequencies lower than the ones detected as corresponding to natural frequencies, these correspond to RBM oscillations for the out-of-plane spectra. As for the in-plane spectra, they are due to interference of the out-of-plane mode shapes, that were still measured by the sensor placed at an in-plane direction. This last phenomenon emphasizes the fact there is human error involved in impact hammer testing and in the sensor placement process. Getting the direction of the hammer to be exactly the same as the one the sensor is facing at every single measurement is virtually impossible, specially with sensors as sensitive as the ones used.

Table 5: Modal parameters for EMA mode shapes.

Mode #	f_{EMA} (Hz)	ζ_{EMA} (%)
1	23.0	2.34
2	41.3	0.647
3	69.8	2.07
4	76.9	1.32
5	102	0.726
6	123	0.916
7	126	0.714
8	133	0.586
9	146	0.900
10	158	0.916

Nevertheless, this kind of results are satisfactory and do not compromise any study that should follow. As long as the modal analysis peaks are filtered and selected conscientiously, valid results can be expected.

The mode shapes were obtained and animated with *MEscope*. All first symmetric and anti-symmetric bending and torsion modes appear and can be seen clearly.

The wing's model updating study could now follow but a similar one has already been done for the BA wing on the previous chapter of this study.

5. Ground Vibration Testing

Preparations for GVT included analyzing the previously developed FEM of the aircraft and consequently the choosing of locations where the sensors were to be placed. *MEscope*'s model was developed before the tests so that the FRFs could be added to the software and the experimental mode shapes examined rapidly. This had to be done fast enough to decide whether or not DOFs were to be added and if some of the extractions had to be repeated.

The results from the analytical model predicted a first symmetrical bending mode shape at 5.6Hz and if testing showed that the first elastic mode was actually substantially lower than that, it could have been critical to some of the control algorithms of the aircraft's autopilot.

The overall procedure required performing two different testing sessions. The need for both of them, their procedure and the results obtained are discussed throughout the rest of this chapter.

5.1. Assumptions, Equipment and Software

The equipment used for the aircraft's GVT is similar to that used on the wing specimen experiment.

Some adaptations to better suit this case regarding instrumentation and software used were:

- Four acquisition cards were used instead of one in order to collect data from 15 sensors and the hammer simultaneously.
- Given the extra mass and inertia of the aircraft when compared to the wing specimen, an extra mass was added to the impact hammer.
- The model generated through *MEscope* was a simplified representation of the aircraft — Fig.3.

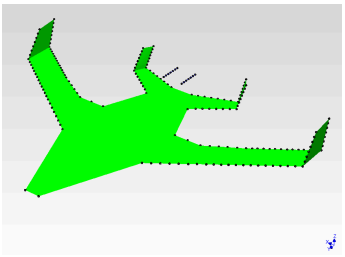

Figure 3: *MEscope* model for the aircraft.

- The DOFs chosen to hit the hammer on were marked with a whiteboard marker.
- The nacelles of the aircraft were only tested in one direction, making use of the fin above them to mark the DOFs.
- Hanging it by a cable was chosen to simulate the free-free boundary condition. This time two cables were used, elevating the aircraft from its supports for Test #1. As for Test #2, the aircraft was supported by one cable alone, elevating it 5cm above the ground.
- The *Labview* interface used for the wing specimen test was improved to acquire the data from 15 sensors and the impact hammer simultaneously.
- A previously developed FEM of the assembled aircraft was used to predict which mode shapes would be detected and at what frequency.

5.2. Test #1

Test #1 was the most extensive one. A total of 186 locations were marked across the aircraft over the wings, winglets, horizontal stabilizer, vertical stabilizers and nacelles. After analyzing the FEM, the wings, winglets and the horizontal stabilizer were decided to be studied for in-plane vibrations as well, corresponding to an overall of 230 DOFs.

By hanging the aircraft from the ceiling by two cables, it rose from the styrofoam supports and an equilibrium position was reached once supported by the cables under tension.

No FRFs were measured at these DOFs and for that reason *MEscope*'s capabilities had to be used to interpolate their displacement on the mode shapes.

Each successful group of three hits in any of the aircraft's structure resulted in 15 FRFs saved. The extractions were considered to be successful if the coherence between the three hits were above 0.9 for the range of interest.

Once the extraction of all FRFs was complete, the computational work of attributing each of the FRFs to the *MEscope* model could be done.

5.2.1 Test #1 Results

The results obtained for the first seven resonant frequencies are presented in Table 6. The relative differences between these and the results obtained using a FEM were also computed.

Table 6: Computational and experimental natural frequencies.

Mode #	f_{FEA} (Hz)	f_{EMA_1} (Hz)	Δf (%)
1	5.57	6.68	+19.93
2	9.00	10.27	+14.11
3	13.97	14.48	+3.65
4	17.82	20.59	+15.54
5	21.95	23.47	+6.92
6	27.23	24.60	-9.66
7	29.87	25.67	-14.06

The aircraft appears to be generally stiffer in bending and torsion when compared to the FEM according to the differences obtained for the natural frequencies. In fact, the FEM went through several mass updates as the development phase of the aircraft progressed but its stiffness did not suffer a final adjustment once the aircraft was assembled, which explains this shift on the lower resonant frequencies.

5.3. Test #2

Once mode shapes were identified there was still the uncertainty on whether or not the peak appeared on the FRF spectra for a frequency slightly bellow the 6.88Hz mode shape was actually an RBM oscillations and not elastic deformation and for this reason, a second testing session was performed.

Overall a simpler test, the number of spots marked on the aircraft this time was reduced to 29. Once again hanging from the ceiling, this time the aircraft was supported by one single cable at a closer position relatively to the ground. This was predicted to shift the RBM oscillations and not in-

terfere with the natural frequencies and would be the most expedite way of confirming if the peaks showing in the FRF spectra for frequencies below 6.68Hz were actually related to RBM.

5.3.1 Test #2 Results

The data collected during Test #2 was later processed and the results compared with the ones obtained for the first testing session.

All of the detected mode shapes happened at a frequency that was within a 2% margin for both testing sessions. Such results show that, as predicted, there was no major shift in these peaks.

As for the question regarding RBM oscillations, the FRF spectra for both tests were also compared visually and then post-processed. With that intent, the frequencies at which the RBM oscillations are detected were computed and are shown in Table 7.

Table 7: Frequencies of RBM oscillations for both tests.

Test #	f_{RBM_1} (Hz)	f_{RBM_2} (Hz)
1	0.59	4.80
2	0.53	3.34

From the results obtained and by animating the RBM peaks, motions resembling pitch and heave behaviors are detected. The first RBM saw its frequency decreased by 11.32% while the second one decreased 43.71% from changing the boundary condition.

Having confidence that the lower frequencies detected in Test #1 are indeed corespondent to RBM oscillations, one can now be surer that the elastic deformations will not compromise the behavior of the aircraft's avionics system during flight.

6. Aircraft Model Update

An attempt at frequency matching proved to be successful by making use of *FEMtools*. As for the mode shapes, a different approach was tried, using an optimization algorithm developed in *MATLAB*.

6.1. Frequency Matching

Similar to the procedure explained in Chapter 3 for the wing, convergence of frequencies between a simplified FEM created on *Ansys APDL* and the data extracted from GVT was attempted. The generated model was made of 19 different beam sections on the fuselage, 25 describing each wing, 15 for each side of the horizontal stabilizer and 10 for both winglets and each of the vertical stabilizers.

The experimental results, after being extracted from *MEscope* as amplitude and phase for each DOF and each mode shape, had to be converted to their real and imaginary parts and put in a .uff format so that they could be imported to *FEMtools*.

The study focused on out-of-plane mode shapes and disregarded the mode shape identified as in-plane on the horizontal stabilizer at 24.60Hz. For that reason, the mode shape previously coined as #7 is now #6. A comparison between the experimental and analytical natural frequencies before any update is presented in Table 8.

Table 8: Comparison between EMA and FEA natural frequencies before model updating.

Mode #	f_{EMA} (Hz)	f_{FEA} (Hz)	Δ_f (%)
1	6.68	7.71	+15.41
2	10.27	10.44	+1.66
3	14.48	11.68	-19.34
4	20.59	16.49	-19.91
5	23.47	24.32	+3.62
6	25.67	25.99	+1.25

This time, four different attempts to match frequencies were made and the parameters to be updated in each of them were the following:

- Updating of E.
- Updating of ρ.
- Updating of A.
- Updating of I_y and I_z.

Starting the iterative loop with CCABS = 10.2%, *FEMtools* converged to 0.88% when updating E alone after seven iterations and having 139 DVs to update the values of. This satisfied the required constraint of having CCABS lower than 1% better than any of the other sets of parameters and for this reason it was found to be enough for satisfactory results when wanting to match frequencies and all FEM's resonant frequencies are now within a margin of 1.5% of the correspondent experimental natural frequencies.

The DVs suffered the biggest updates in the fuselage elements, followed by the horizontal stabilizer and wings. Both winglets and vertical stabilizers saw their first elements — the ones closer to the horizontal stabilizers and the wings respectively — change much more than all their others.

6.2. Mode Shape Matching

As an attempt to develop a more methodic way to converge mode shapes between experimental and analytical data, the mode shape matching was approached by an optimization algorithm developed in *MATLAB*. As many other optimization problems, this one can be generically formulated as follows:

$$\begin{aligned} \text{Minimize} \quad & f(\mathbf{x}) \\ \text{w.r.t.} \quad & \mathbf{x} \in \chi, \\ \text{subject to} \quad & g_i(\mathbf{x}) \leq 0, \ i = 1, ..., m \\ & h_j(\mathbf{x}) = 0, \ j = 1, ..., l\,. \end{aligned} \tag{7}$$

where $\mathbf{x} = [x_1, x_2, ..., x_n]^T$ is the column vector of real-valued design variables and is member of the feasible set of design points χ, f is the objective function to be minimized and $\mathbf{g}$ and $\mathbf{h}$ are the vectors of inequality and equality constraints respectively. To accomplish that, *MATLAB*'s *fmincon* function was used and lower and upper bounds established to constrain the DVs of the generated models in *Ansys APDL*.

From equation 4, it is evident the need of extracting the modal vectors from both analytical and experimental mode shapes before the MAC could be computed. Once done, the model updating study proceeded with an initial attempt at matching the 1st out-of-plane symmetric bending mode shape.

No equality constraints were imposed but the natural frequencies of the FEM were constrained to an interval centered on the EMA's resonant frequencies of the corresponding experimental mode shapes with a maximum deviation of 10%.

6.2.1 1st out-of-plane symmetric bending mode shape

To begin with, the 1st out-of-plane symmetric bending mode shape is attempted to converge. A higher complexity model was generated comparatively to the one used for frequency matching where MPC elements were added to the FEM in order to connect the nodes along the beams to the nearest points where the experimental DOFs were located. Adding to that, the cross section of the beam elements is now tubular rectangular. A total of 17 design variables were chosen and were updated. The best outcome was obtained after 115 iterations for a MAC of 45.57%, an increase of 35.52% from the initial value.

The MAC was computed by extracting the modal vectors from the nodes at the end of each of the generated MPC elements. By comparing these with the corresponding modal vectors from the experimental DOFs through equation 4, *fmincon* was able to minimize the value of $-\text{MAC}_1$.

Though the MAC between experimental and analytical mode shapes increased, results below 60% are usually not satisfactory enough to assume consistency between two mode shapes. For that reason, more freedom was given to the FEM model as an attempt to improve results.

This time, masses were place at the end of the MPC elements and a linear distribution of masses simulated for the wing between the root and kink and between the kink and tip and for the winglet, horizontal and vertical stabilizers between the root and tip.

The structural changes these masses induced put the MAC at a value of 86.26% without any model updating — a very satisfactory value taking into account the starting value of 35.10%. After running the algorithm this increased and converged to an even higher value of 94.09%.

Both undeformed — white — and deformed — blue — configurations can be seen in Fig.4 for $\text{MAC}_1 = 94.09\%$.

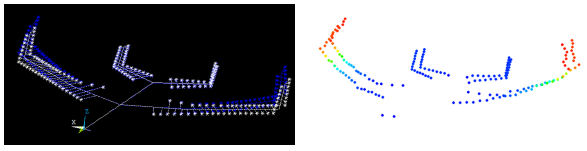

(a) FEM mode shape #1 after addition of masses — isometric view.

(b) EMA mode shape #1 — isometric view.

Figure 4: 1st out-of-plane symmetric bending mode shape.

6.2.2 1st torsion mode shape

The next step in the study was the matching of the 1st torsion mode shape. After some unsuccessful tries, extra DVs were added to the formulation of the problem, increasing the complexity of the FEM. This time, the direction of the masses was uncoupled and DVs #18 to #27 were now used as mass DVs on the x direction while 10 new DVs — DVs #36 to #45 — were used as mass DVs on the y direction. For z direction, the distribution was maintained constant at the value that maximized MAC for the 1st out-of-plane symmetric bending mode shape.

Starting with a MAC equal to 14.47%, after iteration 53 it reached 65.41%, becoming feasible during the running of the algorithm.

6.2.3 Other attempts

When trying to converge more than one mode shape at a time, little success was achieved.

The optimization of the 1st out-of-plane symmetric bending and the 1st out-of-plane anti-symmetric bending mode shapes simultaneous was able to put the MAC of the former at 89.63% and the latter at 40.55%, an average increase of 38.58% from initial MAC conditions. However, the frequency margin could not be satisfied, compromising the accuracy of this FEM to describe experimental data.

Another attempt involved both 1st out-of-plane symmetric bending and 1st torsion mode shapes.

This time, feasibility criteria were satisfied but no improvement was obtained on the average MAC of these mode shapes during the time available to devote to this study.

This can indicate that more freedom or a refined version of the FEM should be used if interested in proceeding with this study.

7. Conclusions

The introductory model update study on the GVT data from the aircraft's wing made possible an understanding of how an optimization algorithm can be implemented to match properties between experimental and analytical models. When frequencies were to be matched, *FEMtools* was capable of reducing CCABS from 31.6% to 0.69% by updating E, ρ, A, I_y and I_z. The attempts at mode shape convergence proved to be much more challenging and led to no success.

Preparations for GVT involved developing a *LabView* interface that was used for collecting FRFs of up to 16 sensors simultaneously and the preparation of a *MEscope* model that allowed to compare the analytical results with the ones obtained from experience as efficiently as possible.

Overall successful, by performing two test sessions, RBMs were identified and the first elastic mode shape found at 6.68Hz, which indicates an apparently stiffer wing than the one predicted analytically.

The model update study followed firstly for frequency matching by making use of *FEMtools*' capabilities and finally for mode shape matching through an optimization algorithm developed in *MATLAB*. For the former, by updating E alone on a FEM made of beam elements to simulate the aircraft behavior. As for the latter, more complex FEMs were generated and lead to the convergence of the 1st out-of-plane symmetric bending mode shape and to a significant increase in the MAC of the 1st torsion mode shape of the wings. Nonetheless, when trying to converge multiple mode shapes at once, the algorithm showed to be incapable of solving the problem, demonstrating there is room for adjustment and improvement on both the FEMs and the algorithm itself.

7.1. Future Work

From the work presented on this document, a series of ideas on what could follow this study are presented:

- **Optimization algorithm**: Taking advantage work developed here, a broader convergence between the simplified FEM mode shapes and the experimental ones can be attempted so that the dynamic behavior of the aircraft can be represented as accurately as possible.
- **Structural analysis**: The mode-superposition method can be applied to characterize the response of the aircraft to transient excitations.
- **Flutter analysis**: An aeroelastic flutter analysis can be performed once the dynamic behavior of the simplified FEM mimics experimental results.
- **Aeroservoelatic model**: Following the flutter analysis, an aeroservoelastic model can be derived to actively suppress flutter.

Acknowledgements

My words of gratitude go towards my supervisors, Professor Afzal Suleman and Doctor José Vale for their guidance and help and my family and close friends for all the unconditional support.

References

[1] Clayton Humphreys-Jennings, Ilias Lappas, and Dragos Mihai Sovar. Conceptual design, flying and handling qualities assessment of a blended wing body (bwb) aircraft by using an engineering flight simulator, April 2020. School of Engineering, University of South Wales.

[2] R. H. Liebeck. Design of the blended wing body subsonic transport. *Journal of Aircraft*, 41(1):10, January 2004. doi:10.2514/1.9084.

[3] Crystal Instruments. Basics of modal testing and analysis. https://www.crystalinstruments.com/basics-of-modal-testing-and-analysis, 2017. (accessed on May 17th 2021).

[4] Agilent Technologies. The fundamentals of modal testing. Technical report, Agilent Technologies, 2000. Application Note 243-3.

[5] George A. Papagiannopoulos and George D. Hatzigeorgiou. On the use of the half-power bandwidth method to estimate damping in building structures. *Soil Dynamics and Earthquake Engineering*, 31:1075–1079, February 2011.

[6] Randall J. Allemang. The modal assurance criterion - twenty years of use and abuse, August 2003. University of Cincinnati, Ohio.

[7] FEMtools, Interleuvenlaan 64 - 3001 - Leuven - Belgium. *FEMtools Model Updating Theoretical Manual*, 4.1.2 edition, mar 2020.

[8] Gonçalo Araújo. Model updating based on static and ground vibration tests of a blended wing body aircraft. Master's thesis, Instituto Superior Técnico, 2021.